Title
A MICROSCOPIC CALCULATION OF FRAGMENT FORMATION IN NUCLEUS-NUCLEUS COLLISIONS

Author
Harvey, B.G.

Publication Date
1984-04-01

Lawrence Berkeley Laboratory
UNIVERSITY OF CALIFORNIA

Submitted for publication

A MICROSCOPIC CALCULATION OF FRAGMENT FORMATION IN NUCLEUS-NUCLEUS COLLISIONS

B.G. Harvey

April 1984

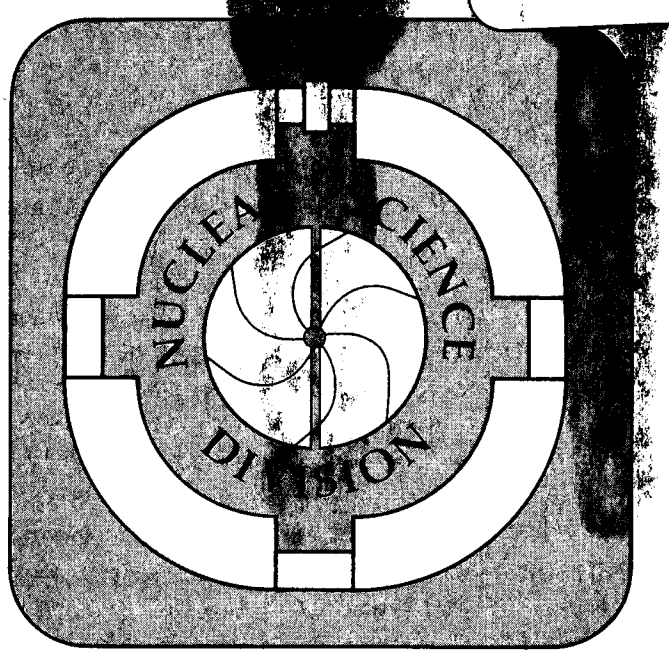

Prepared for the U.S. Department of Energy under Contract DE-AC03-76SF00098

DISCLAIMER

A MICROSCOPIC CALCULATION OF FRAGMENT FORMATION IN NUCLEUS-NUCLEUS COLLISIONS*

Bernard G. Harvey

Nuclear Science Division
Lawrence Berkeley Laboratory
University of California
Berkeley, CA 94720

April 1984

ABSTRACT

A very simple microscopic model using effective nucleon-nucleon cross sections is used to calculate the relative yields of projectile-like fragments from nucleus-nucleus collisions. Good agreement with reaction cross section measurements is obtained. The enhanced yields of neutron-rich fragments from neutron-rich targets observed experimentally at low beam energies are reproduced only by the inclusion of a neutron-rich nuclear surface. Each fragment mass is produced in a strongly localized region of the distance of closest approach between the colliding nuclei.

*This work was supported by the Director, Office of Energy Research, Division of Nuclear Physics of the Office of High Energy and Nuclear Physics of the U.S. Department of Energy under Contract DE-AC03-76SF00098.

I. INTRODUCTION

Soon after beams of heavy ions of 20 MeV/A and 2GeV/A became available from the 88-Inch Cyclotron and the Bevalac at Berkeley, an unexpectedly strong similarity was found between nucleus-nucleus collisions at these two widely different energies[1]. In particular, the yields of projectile-like fragments (PLF), when summed by atomic number, were nearly the same for 20 MeV/A as for 2 GeV/A ions of ^{16}O.

When the target was a heavy nucleus such as ^{208}Pb, there were nevertheless consistent differences in the yields of individual isotopes; the neutron-excess isotopes were produced in much greater yields at 20 MeV/A than at 2 GeV/A. This difference is shown in Table I.

At 20 MeV/A, the yields of neutron-excess fragments were greater from a target of ^{208}Pb than from the less neutron-rich target ^{94}Zr. At 2 GeV/A, though, there was no such effect in the comparison of yields from targets of Cu and Pb. The comparison of yields from ^{20}Ne + ^{197}Au (290 MeV) with those from ^{20}Ne + ^{58}Ni (270 MeV) shows again a large enhancement of the neutron-excess isotopes from the ^{197}Au target[2]. This result has been discussed by Homeyer[3].

Thus it seems reasonably well established that the large extra yields of neutron-rich isotopes at lower energies are associated with large values of the ratio N/Z of the target. At 2 GeV/A, these extra yields are not observed, even from extremely neutron-rich targets.

It is tempting to associate these observations with the behavior of the nucleon-nucleon cross sections shown in Fig. 1. At low energies,

σ_{np} is three times larger than σ_{nn} and σ_{pp}. Therefore, protons from the projectile are more likely to be scattered from target nucleons than are projectile neutrons, when the target has N > Z. The PLF should therefore be proton-deficient and neutron-rich. At ~ 500 MeV (lab) and beyond, σ_{np} becomes approximately equal to σ_{nn} (σ_{pp}) so that the N/Z ratio of the target is no longer of importance. With the further assumption that the removal of nucleons from the projectile to form the fragment occurs only through these N-N scatterings, it is clear that the trends of the N-N cross sections are in the right direction to account qualitatively for the experimental results shown in Table I.

It is by now well established that the drop in the reaction cross section σ_R observed in many colliding systems at energies beyond ~ 20 MeV/A can be quantitatively explained by the energy-dependence of the nucleon-nucleon cross sections[4-8]. The microscopic calculations of refs. 5-7 are extremely elaborate. They take into account the effects of the Fermi motion of the nucleons in the collision partners, as well as the Pauli blocking of elementary scatterings in which one or both of the nucleons remain below the Fermi surface. Nevertheless, calculations without Fermi motion and Pauli blocking gave reasonable values of σ_R even at energies as low as 20 MeV/A[6,8,9]. Therefore it seemed worthwhile to make the simplest possible calculation to see to what extent the N-N cross sections might account for the experimental observations described above.

II. THE CALCULATIONS

The two colliding nuclei are assumed to have spherically symmetric Fermi density distributions. The radius and diffusivity of the neutron distribution can be changed relative to that of protons to allow the use of a neutron-rich surface in heavy target nuclei. The projectile (Z_1,A_1,N_1) follows a Coulomb path with impact parameter b until it touches the target nucleus. The projectile nucleons then follow straight paths into and through the target. The distance of closest approach between target and projectile centers is D. It is assumed that any projectile nucleon that scatters from a target nucleon will be permanently removed from the projectile, and that no target nucleons are scattered into bound states of the PLF. The number of scattered projectile neutrons and protons was calculated by Monte Carlo techniques. For each value of b, 1000-2000 projectiles were allowed to collide. The impact parameter b was successively incremented in 16 steps from 0 to 14 fm, beyond which there were no N-N scatterings.

The geometry of the collison is illustrated in fig. 2. The distance r_1 of the nucleon P from the projectile center was chosen at random in the interval 0-5 fm, well out into the tail of the density distribution for projectiles up to A=20. The projectile density at P was calculated and the choice of r_1 was accepted or rejected in such a way as to reflect the projectile density at P. If it was rejected, another choice of r_1 was made. For an accepted r_1, the angle θ was chosen in the interval $0-\pi$. Then the angle ϕ was chosen in the range $0-2\pi$ and the lengths r and c were computed. The distance R between P and the target center was then obtained from:-

$$R = [(D-r)^2 + (Z-c\cos\theta)^2 + c^2\sin^2\theta]^{1/2} \qquad (1)$$

The target neutron and proton densities at P were then calculated. The length Z was next stepped and the target neutron and proton densities recalculated at each new value of R.

If the projectile nucleon is a proton, the probability that it will not scatter from a target proton or nucleon as it moves along the Z-direction is:

$$P_p = \exp - \left(\int \rho_n(z)\sigma_{pn}(R,r_1)dz + \int \rho_p(z)\sigma_{pp}(R,r_1)dz\right) \quad (2)$$

For a projectle neutron, the corresponding probability is:-

$$P_n = \exp \left(\int \rho_n(z)\sigma_{nn}(R,r_1)dz + \int \rho_p(z)\sigma_{np}(R,r_1)dz\right) \quad (3)$$

Here, $\rho_n(z)$ and $\rho_p(z)$ are the target neutron and proton densities at each point along the trajectory. The subscripts (p or n) on the cross sections refer in order to the projectile nucleon and the target nucleon. As discussed below, the effective nucleon-nucleon cross sections were allowed to vary with the distances R and r_1 of the projectile nucleon from the target and projectile centers. The integrals were evaluated by Simpson's rule in ten intervals of Z from 0 to + 14 fm and then doubled to obtain their values from -14 to +14 fm.

For each probability P_p or P_n, a decision was made as to whether or not a scattering ocurred by generating a random number N in the interval 0-1/P. If $N \geqslant 1$, a scattering was assumed to have happened. This procedure was repeated N_1 times (neutrons) and Z_1 times (protons) to obtain the number of protons and neutrons scattered out of

the projectile, and hence the numbers Z_3 and N_3 remaining in the PLF. This was then repeated 1000-2000 times from each value of b.

III. RESULTS

1. REACTION CROSS SECTIONS

Since Pauli blocking is not included in the calculation, the values of σ_{nn} and σ_{np} at the lower energies have to be treated as parameters whose values ought to be smaller than the free N-N scattering cross sections, but with the ratio σ_{nn}/σ_{np} about equal to that of the free N-N values. If Pauli-blocked values of σ_{nn} and σ_{np} are chosed to be 6.5 and 23 mb at 10 MeV/A (CM), corresponding to a mean free path of 4 fm [10-12] in nuclear matter of density of 0.17 nucleons/fm^3, the values of σ_R that are obtained are substantially lower than experiment.

It is well known[7] that Pauli blocking should be reduced in the nuclear surface. Using the Reid hard-core potential, Jeukenne et al.[13] found that the value of W_0/ρ varied approximately as $1/\rho$ for projectiles of 10-50 MeV. Here W_0 is the isoscalar component of the optical model potential. Since $W_0/\rho \propto \sigma_{NN}$, this result suggests that σ_{NN} should be roughly proportional to $1/\rho$. At 140 MeV, W_0/ρ was found to be almost independent of ρ so that σ_{NN} should be constant throughout the nuclear volume. For low energy projectiles, absorption is mainly in the nuclear surface, while above about 50 MeV[13] it occurs throughout the volume.

The detailed calculations of DiGiacomo et al.[7] show that the effective N-N cross sections reach the free values for projectile nucleons of only 20 MeV in the surface region where $k_F = 0.5$ fm^{-1}. This value of k_F corresponds to a density of about 5 of the central

value. For projectile energies > 150 MeV, the effective cross sections are very nearly equal to the free values at all values of k_F and hence independent of the density.

These results suggested a very simple approximation for the radial dependence of the effective cross sections for 20 MeV/A projectiles. In the central region, σ_{nn} and σ_{np} were given values corresponding to a nucleon mean free path in the range 2-4 fm, with the ratio σ_{np}/σ_{nn} equal to 3, the ratio for the free N-N cross sections. The cross sections varied as $1/(\rho_1\rho_2)^{1/2}$ up to the free values, ρ_1 and ρ_2 are the neutron or proton densities in the target and projectile nuclei. Thus the effective cross sections became functions of R and r_1 in eqs. 2 and 3. At 2 GeV/A on the other hand, the Pauli blocking should have a negligible effect even in the center region. The free N-N cross sections were therefore used throughout the nuclear volume.

This procedure immediately revealed that, as might be expected, the reaction cross sections σ_R are sensitive only to the N-N cross sections in the surface region, while the "complete fusion" cross sections are sensitive mainly to their values in the interior. Here, a "complete fusion" event is defined as one in which every projectile nucleon scattered. Only at the lowest energies are all these scattered projectile nucleons likely to be absorbed in the target. For example, in the system $^{12}C+^{12}C$, the use of free N-N cross sections throughout the target nucleus volume gave σ_{fus} of 311 mb at 10 MeV/A (CM) whereas the variable cross section method gave 47 mb, a much more plausible value.

Similar results were obtained for $^{16}O + ^{208}Pb$ at 20 MeV/A (lab). In both systems, σ_R was exactly the same for both procedures. Unfortunately, complete fusion cross sections are very difficult to measure at energies beyond 20 MeV/A where the present Monte Carlo calculations are most likely to have some validity. Comparison with experiment is therefore not possible.

The reaction cross section was obtained by summing all events in each area $2\pi b\, db$ in which at least one projectile nucleon was scattered. Figure 3 shows a comparison of calculated and experimental values of σ_R for the system $^{12}C + ^{12}C$. Free N-N cross sections were used in the surface region at all energies. The calculated values of σ_R are in excellent agreement with experiments.

2. N/Z RATIOS IN EJECTILES

Table I summarizes some typical results. The first column shows the experimental ratios of PLF production cross sections for $^{16}O + ^{94}Zr$ and $^{16}O + ^{208}Pb$ at 20 MeV/A[1]. The second column shows the calculated values of the same ratios using σ_{nn}, σ_{np} of 15.6, 46.9 mb in the target center, i.e. a mean free path of 2 fm. The ratio of neutron/proton densities was assumed to be constant even out into the tail of the target nucleus matter distribution. The cross sections were allowed to increase from their central values as $1/\rho_n$ or $1/\rho_p$, up to 280, 849 mb. The calculation gives no enhancement of the neutron-rich PLF's from the ^{208}Pb target.

The third column of Table I shows the results of a calculation using the same cross sections in which the radius of the neutron distribution in ^{208}Pb was increased relative to the proton distribution by 0.20 fm[14]. The neutron and proton diffusivities were 0.558 and 0.455 fm[15]. The parameters used for ^{208}Pb closely reproduce the ratios of neutron to proton densities from 8 to 12 fm measured by Körner and Schiffer[16]. For ^{94}Zr, the neutron radius increase was 0.07fm[14] and the neutron and proton diffusivities were 0.569, 0.501 fm[15]. These parameters give ρ_n/ρ_p slightly smaller than N/Z in the central region, but much larger than N/Z in the low-density tail, especially in ^{208}Pb. Now, there is a clear enhancement of the yields of neutron-rich PLF's from ^{208}Pb. As fig. 4 shows, the calculated ratios agree remarkably well with experiment.

The fourth column of Table I shows the experimental ratios of PLF yields from ^{16}O + ^{208}Pb at 20 MeV/A and 2 GeV/A[1]. The fifth column shows the calculated ratios for identical neutron/proton density distributions in ^{208}Pb. At 20 MeV/A, σ_{nn}, σ_{np} were set equal to the values given above. At 2 GeV/A, the cross sections were 50, 45mb at all radii. Again, there is only a small enhancement of neutron-rich PLF yields at 20 MeV/A.

The sixth column shows the effect of including a neutron skin in ^{208}Pb, using the parameters mentioned above. There is a clear enhancement of the yields of neutron-rich PLF's at 20 MeV/A, but still less than is observed experimentally. The inclusion of target nucleons

that scatter into bound states of the PLF might further increase the yields of neutron-rich ejectiles from ^{208}Pb at 20 MeV/A but should have little effect at 2 GeV/A.

The neutron-rich enhancements depend upon two separate and distinct factors. First, the heavy ion energy must be low enough that $\sigma_{np} > \sigma_{nn}$. Second, the effective cross sections must increase substantially with radius so that they reach large (essentially free) values in the low density tail of the nuclear matter distribution where the ratio of neutron to proton densities is very much larger than N/Z. A large value of N/Z without a neutron-rich skin is not by itself enough to produce a noticeable enhancement.

The present exploratory calculations perhaps justify the effort required to modify the methods of e.g. ref. 7 to include separate neutron and proton density distributions. If that were successful, the accurate measurement of PLF yields from heavy ion reactions at 20-100 MeV/A might become a valuable new tool for the study of the composition of nuclear surfaces.

3. SPATIAL LOCALIZATION OF THE REACTIONS

The overlap model[17] is extremely successful in predicting elemental yields from heavy ion reactions. Its primary assumption is that the nucleons that are removed from the projectile to form a given PLF must overlap in space with the target nucleus. For each PLF mass

there is an optimum distance of closest approach D(i) at which the appropriate overlap is obtained. Light fragments come from collisions with a small value of D(i), heavy ones from large values of D(i). The probability P(i) of forming the ith PLF mass varies with D around the optimum value of D(i) according to:-

$$P(i) = \frac{D - D(i) + \sigma}{\sigma^2} \exp - \left(\frac{D - D(i) + \sigma}{\sigma}\right) : D > D(i) - \sigma \qquad (4)$$

$$= 0 : D \leqslant D(i) - \sigma$$

The value of σ was adjusted to obtain the best agreement with experimental cross sections. The value of 0.65 fm thus found corresponds to a full width at half maximum of about 1.6 fm. Thus the localization is quite sharp, as shown in fig. 5. The colliding nuclei were $^{16}O + ^{208}Pb$ at 20 MeV/A.

The Monte Carlo calculations also show a strong localization of the distances of closest approach at which the various PLF's are made. A typical result is shown in fig. 6 for the collision of ^{16}O and ^{208}Pb at 20 MeV/A. The σ_{nn} and σ_{np} cross sections were set equal to the free values at all radii to simulate the "black nucleus" assumption of the overlap model. Using low central cross sections that rise to the free values in the surface gives very similar results: the ^{12}C and ^{15}N peaks move to radii larger by 0.5 fm. The relative heights of the peaks reflect the number of ways in which the nucleons can be divided between protons and neutrons. Thus to make a PLF of mass 15, either a proton or a neutron must scatter. For

PLF's of mass 1, there are also just two choices: it must be either a proton or neutron that escapes. For mass 8, though, many combinations of N and Z summing to 8 are possible: ^{8}Be is just one of them. The peak areas reflect the "spectroscopic factor" of Friedman's fragmentation model[18].

The remarkable similarity between figs. 5 and 6, extending even to the widths of the peaks, strongly supports the sharp localization that is the central assumption of the overlap model.

IV. SUMMARY OF CONCLUSIONS

A very simple microscopic calculation reproduces the energy dependence of reaction cross sections, provided that free nucleon-nucleon scattering cross sections are used in the low density tail of the nuclear matter distribution. Calculated σ_R values are very insensitive to the N-N cross sections in the nuclear interior .

The calculations using a neutron-rich skin reproduce quite well the enhanced yields of neutron-rich fragments that are observed from heavy element targets at 20 MeV/A. Without the neutron skin, only a small enhancement coming from the large N/Z ratio is obtained.

The distances of closest approach at which the various mass fragments are made are found to be strongly localized. Light fragments are formed at small distances and heavier ones at larger distances. This result lends strong support to the assumptions that were made in the overlap model[17].

ACKNOWLEDGEMENTS

The author thanks R. G. Stokstad for invaluable critical comments, W. D. Myers and J. Treiner for helpful discussions of neutron skins and S. B. Gazes for many suggestions on a wide variety of topics.

Table I. Fragment yield ratios for $(^{16}O+^{94}Zr)/(^{16}O+^{208}Pb)$, 20 MeV/A and $(^{16}O+^{208}Pb$, 20 MeV/A$)/(^{16}O+^{208}Pb$, 2 GeV/A). Experimental values from Ref. 1. See text for parameters used in calculations. Columns headed CALC I (CALCII) were made without (with) a neutron skin. Calculated values in parentheses are based on $\leq$ 50 Monte Carlo events.

Fragment	$\frac{\sigma(^{16}O+Zr)}{\sigma(^{16}O+Pb)}$			$\frac{\sigma(^{16}O+Pb)\ 20\ MeV/A}{\sigma(^{16}O+Pb)\ 2\ GeV/A}$		
	EXPT	CALC I	CALC II	EXPT	CALC I	CALC II
^{6}Li	0.95	1.0	0.96	1.0	1.0	1.3
^{7}Li	0.73	0.94	0.80	2.4	0.97	1.4
^{8}Li	-	0.80	0.83	-	(2.0)	1.7
^{9}Li	-	1.1	0.80	-	(1.4)	3.7
^{7}Be	1.3	1.0	1.3	0.45	1.1	0.79
^{9}Be	0.85	0.89	0.84	3.5	1.4	1.4
^{10}Be	0.75	0.91	0.77	6.0	1.4	1.8
^{11}Be	-	-	0.49	-	(1.8)	2.9
^{9}B	-	1.1	1.2	-	1.0	0.80
^{10}B	1.2	1.0	1.1	1.6	1.4	0.91
^{11}B	1.0	0.97	0.86	2.2	1.1	1.5
^{12}B	0.80	0.73	0.67	6.0	1.6	1.7
^{13}B	-	1.1	0.79	-	(1.7)	2.9
^{11}C	1.6	1.1	1.1	0.75	1.1	1.0
^{12}C	1.3	1.1	1.1	1.6	0.95	1.1
^{13}C	0.83	0.88	0.86	2.8	0.97	1.3
^{14}C	1.0	0.99	0.78	3.5	1.4	1.5
^{13}N	1.0	1.0	1.2	1.7	1.2	0.69
^{14}N	0.80	0.94	0.92	2.0	1.1	1.1
^{15}N	0.66	0.89	0.83	-(1)	1.1	1.4

(1)The ^{15}N yield at 2 GeV/A contains a large photonuclear component.

REFERENCES

1. G. K. Gelbke et al., Physics Reports 42 No 5 312 (1978).

2. Ch. Egelhaaf, Thesis, Hahn-Meitner Institut, Berlin (1982).

3. H. Homeyer, Nuclear Science Research Conference Series, Vol. 6 p. 95, "Nuclear Physics with Heavy Ions", Harwood Academic Publishers, 1984.

4. R. M. DeVries and J. C. Peng, Phys. Rev. Lett. 43 1373 (1979).

5. N. J. DiGiacomo, R. M. DeVries and J. C. Peng, Phys. Rev. Lett. 45 527 (1980).

6. R. M. DeVries and J. C. Peng, Phys. Rev. C22 1055 (1980).

7. N. J. Di Giacomo, J. C. Peng and R. M. DeVries, Phys. Lett. 101B 383 (1981).

8. J. C. Peng, R. M. DeVries and N. J. DiGiacomo, Phys. Lett. 98B 244 (1982).

9. H. Bertini, Phys. Rev. C5 2118 (1973).

10. J. W. Negele and K. Yazaki, Phys. Rev. Lett. 47 71 (1981).

11. B. Sinha,Phys. Rev. Lett. 50 91 (1983).

12. J. W. Tanahata et al., Phys. Lett. 100B 121 (1981).

13. J. P. Jeukenne, A. Lejeune and C. Mahaux, Phys. Rev. C 16 80 (1977).

14. J. W. Negele and D. Vautherin, Phys. Rev. C5 1472 (1972).

15. F. Tondeur, J. P. Arcoragi and J.M. Pearson, Contribution to the International Workshop on Semiclassical Methods in Nuclear Physics. Institut Laue-Langevin, Grenoble, 1984.

16. H. J. Körner and J. P. Schiffer, Phys. Rev. Lett. 27 1457 (1971).

17. B. G. Harvey and H. Homeyer, LBL Report 16882, to be submitted to Phys. Lett.

18. W. A. Friedman, Phys. Rev. C 27 569 (1983).

FIGURE CAPTIONS

Fig. 1. The free N-N total cross sections.

Fig. 2. The collison geometry used in the Monte Carlo calculations.

Fig. 3. Comparison of Monte Carlo calculations using free N-N cross sections in the surface (●) witn experimental measurements (o) of σ_R for $^{12}C + ^{12}C$. The dashed line is the Glauber model calculation of Ref. 8.

Fig. 4. Fragment yield ratios $(d\sigma/d\ ,^{16}O + ^{94}Zr)/(\sigma,\ ^{16}O + ^{208}Pb)$ at 20 MeV/A(lab). The experimental values are from Ref. 1. The lines connect the calculated values from Table I. Parameters used are given in the text.

Fig. 5. Spatial localization of fragment sources for $^{16}O + ^{208}Pb$ at 20 MeV/A. Calculations from overlap model of Ref. 17.

Fig. 6. Spatial localization of fragment sources for $^{16}O + ^{208}Pb$ at 20 MeV/A. Monte Carlo calculations.

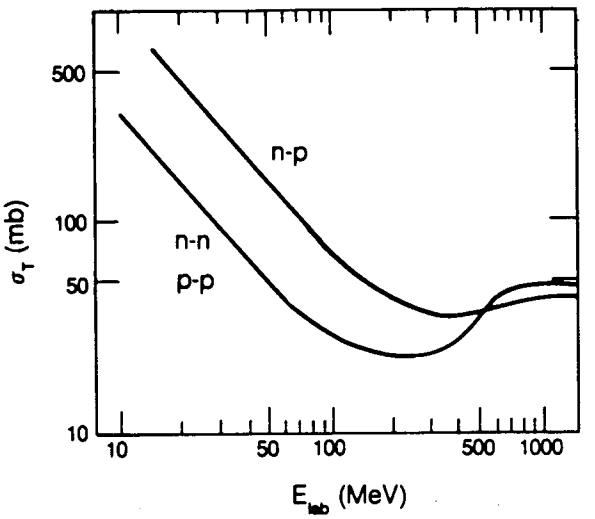

Fig. 1

XBL 844-9327

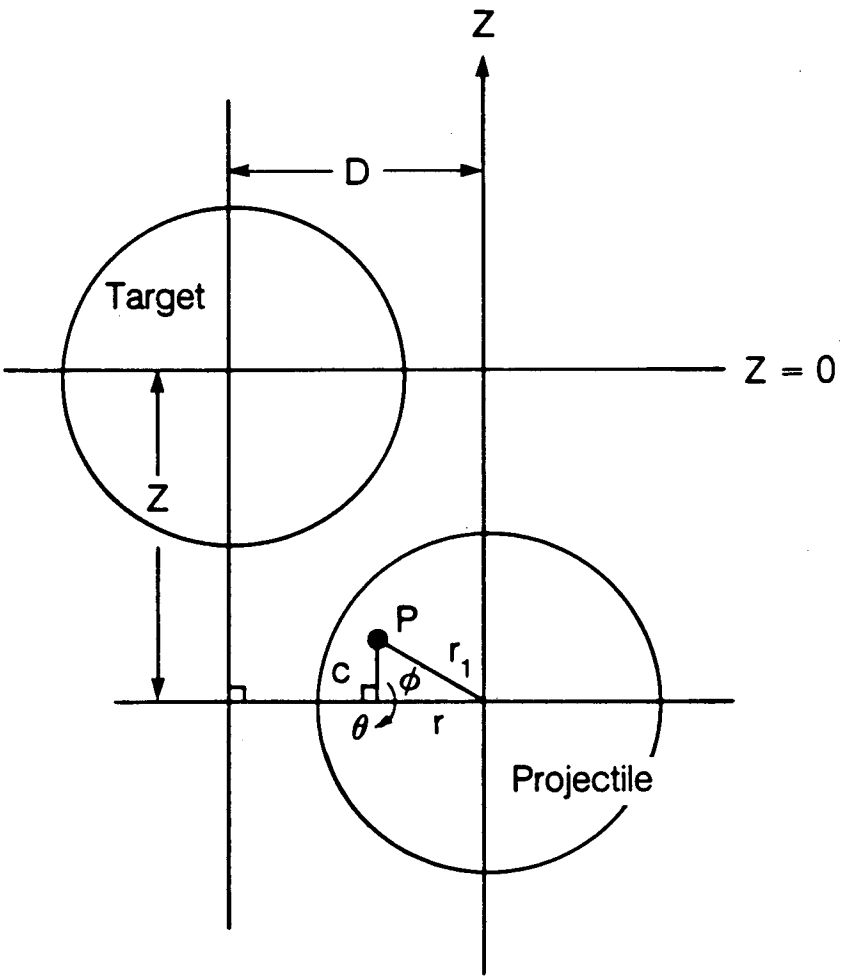

Fig. 2

XBL 844-9324

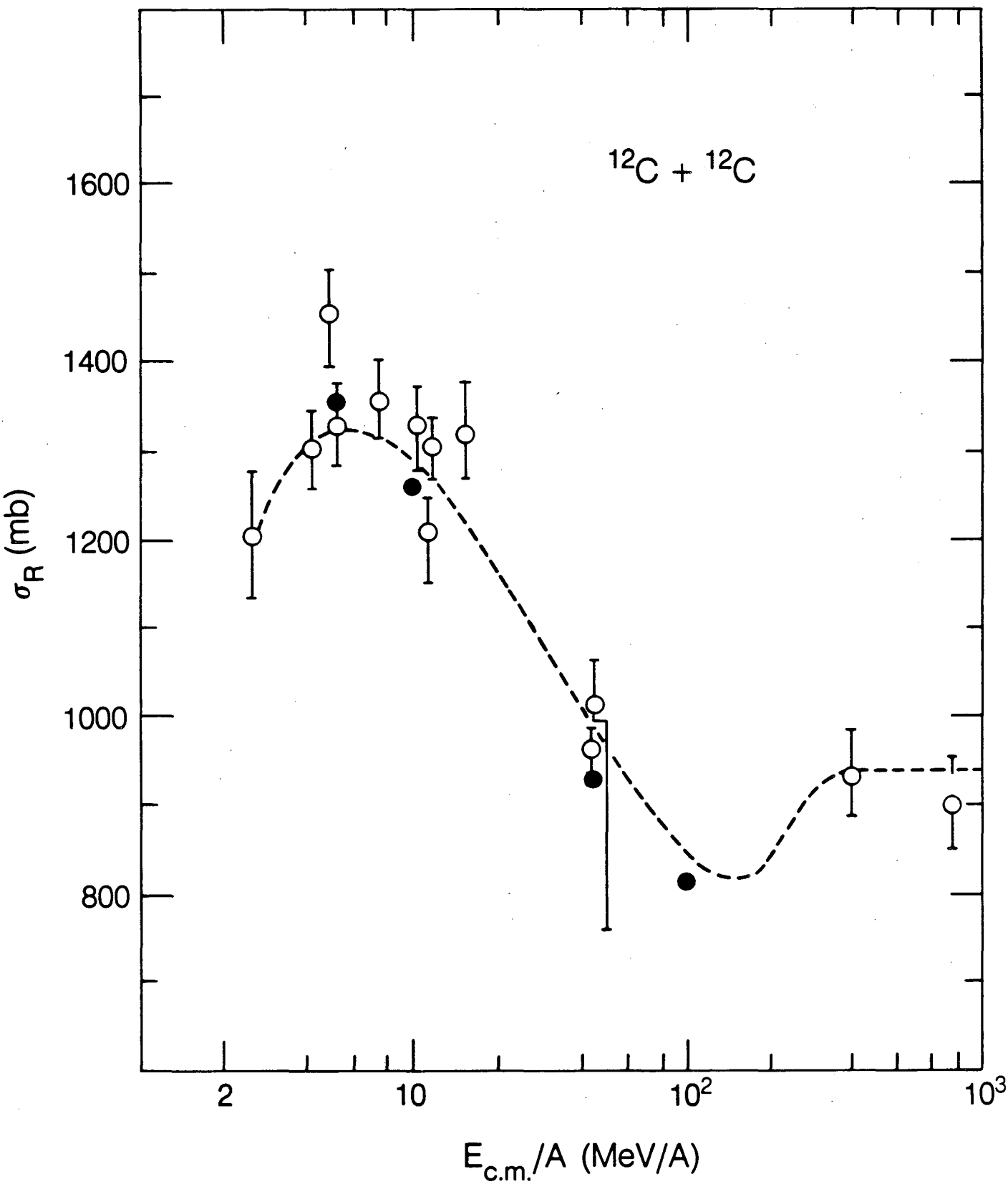

Fig. 3

XBL 844-9325

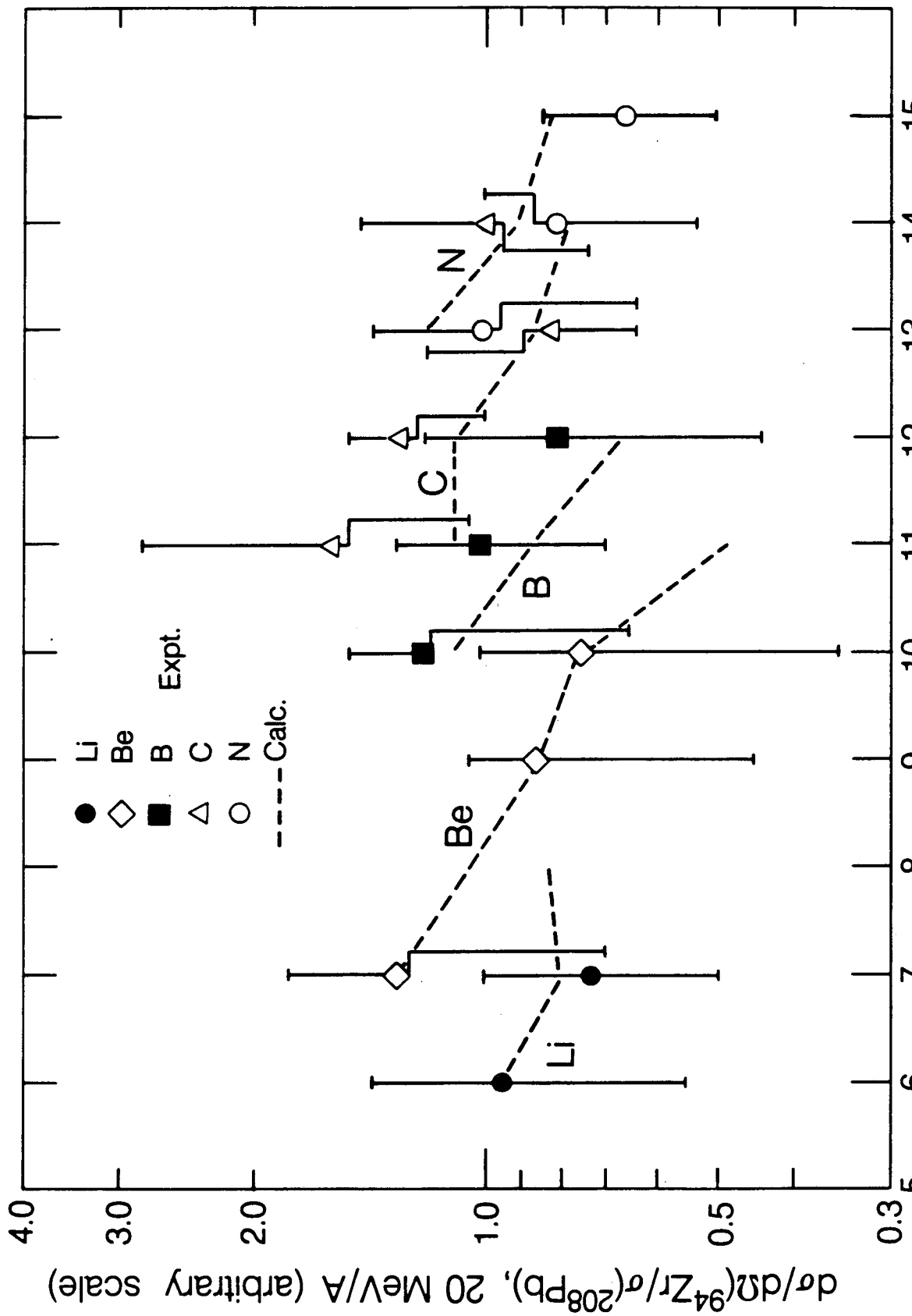

XBL 844-9326

Fig. 4

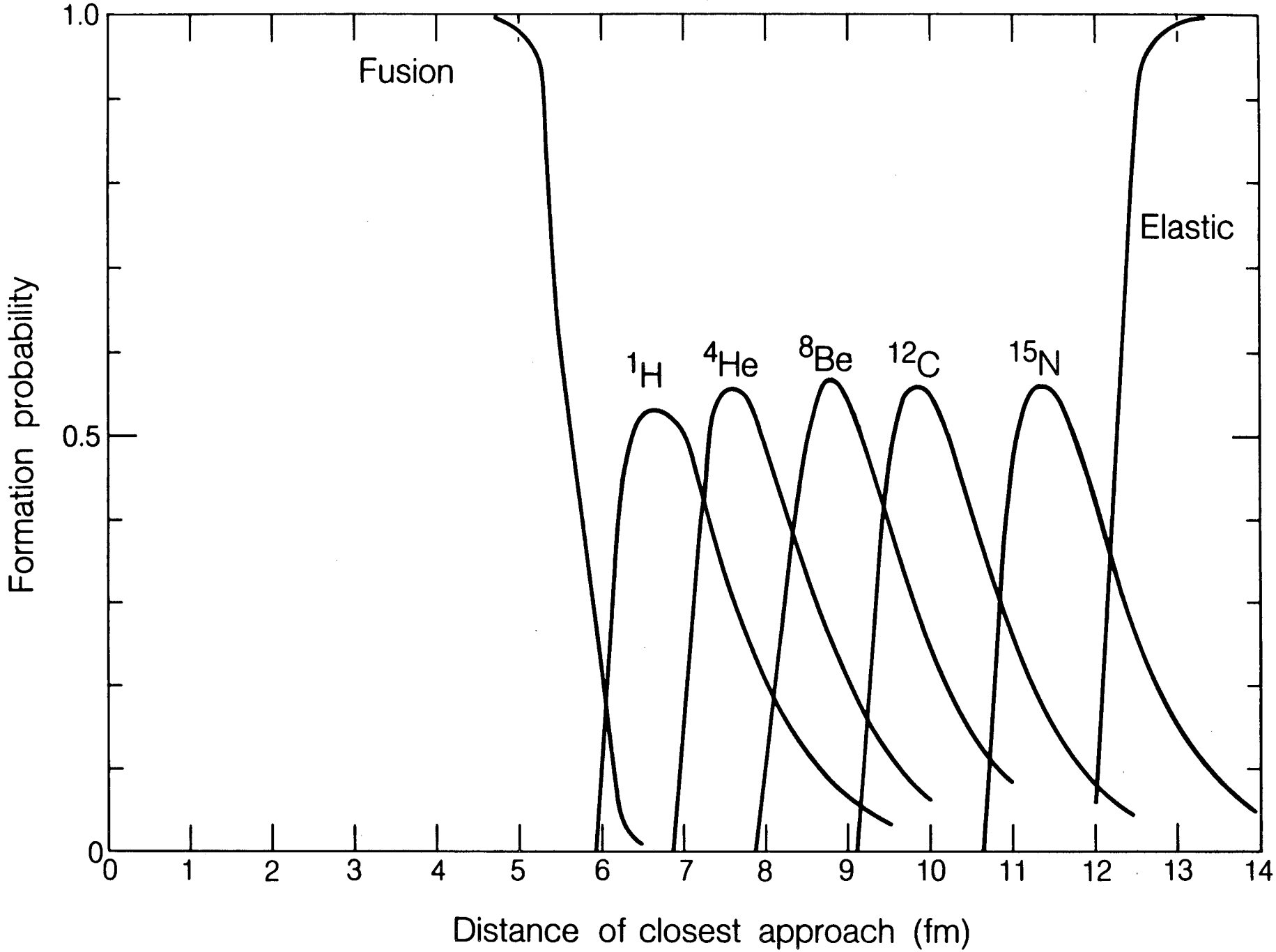

XBL 844-9328

Fig. 5

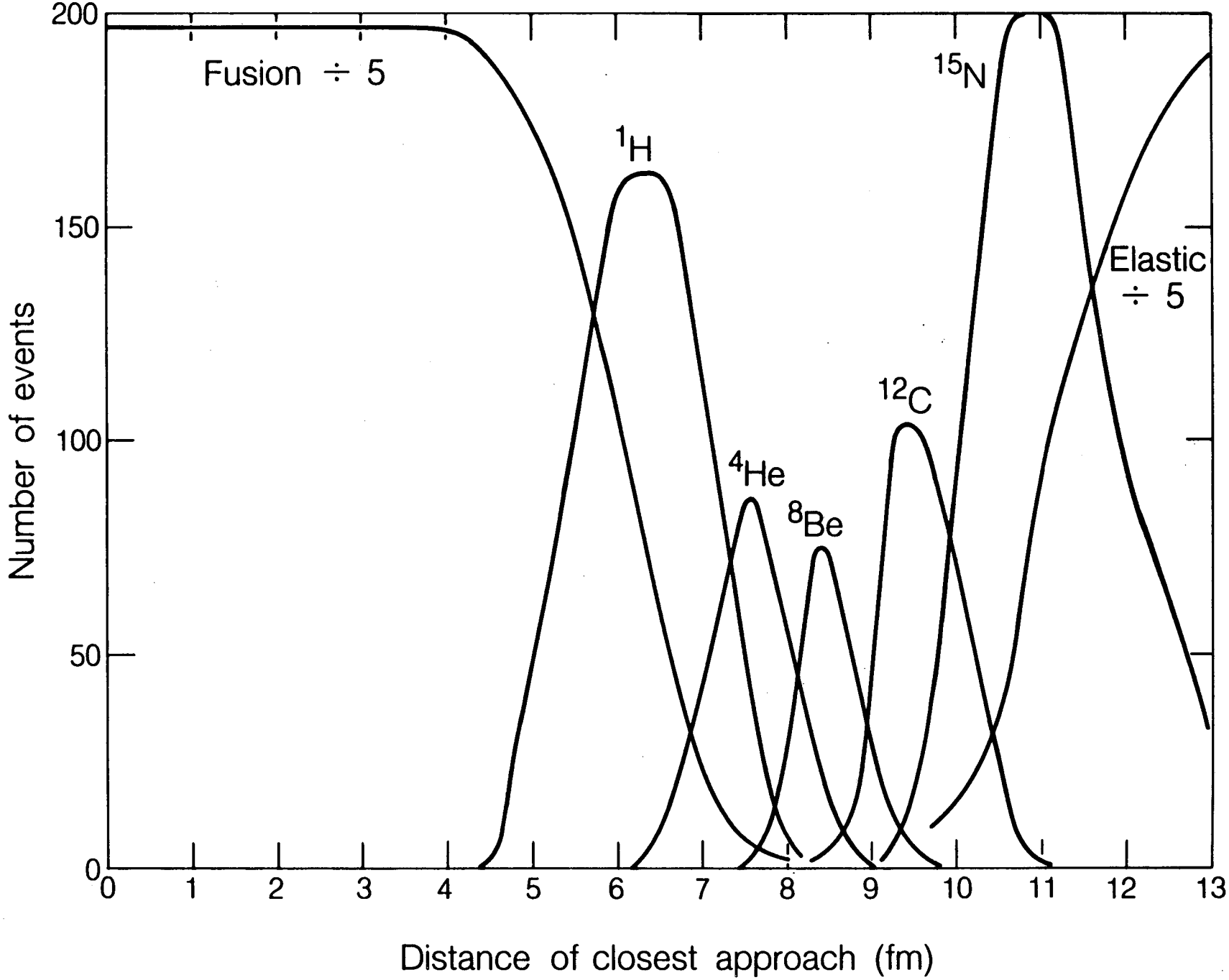
200
150
100
50
0
Number of events
Fusion ÷ 5
^{1}H
^{15}N
Elastic
÷ 5
^{12}C
^{4}He
^{8}Be
0 1 2 3 4 5 6 7 8 9 10 11 12 13
Distance of closest approach (fm)

XBL 844-9329

This report was done with support from the Department of Energy. Any conclusions or opinions expressed in this report represent solely those of the author(s) and not necessarily those of The Regents of the University of California, the Lawrence Berkeley Laboratory or the Department of Energy.

Reference to a company or product name does not imply approval or recommendation of the product by the University of California or the U.S. Department of Energy to the exclusion of others that may be suitable.

TECHNICAL INFORMATION DEPARTMENT
LAWRENCE BERKELEY LABORATORY
UNIVERSITY OF CALIFORNIA
BERKELEY, CALIFORNIA 94720